The EUMETSAT Network of Satellite Application Facilities

OSI SAF
Ocean and Sea Ice

Algorithm Theoretical Basis Document for the OSI SAF Global Reprocessed Sea Ice Concentration Product

OSI-409, OSI-409-a, OSI-430
Version 1.1

Steinar Eastwood, Thomas Lavergne and Rasmus Tonboe

7. March 2014

This page is intentionally left blank.

Document Change Record

Version	Date	Change	Description	Responsible
1.0	18.11.2013		First version for review	Steinar Eastwood
1.1	27.02.2014		Updated after PCR review	SE

Table of Contents

1 Introduction

1.1 The EUMETSAT Ocean and Sea Ice SAF

For complementing its Central Facilities capability in Darmstadt and taking more benefit from specialized expertise in Member States, EUMETSAT created Satellite Application Facilities (SAFs), based on co-operation between several institutes and hosted by a National Meteorological Service. More on SAFs can be read from www.eumetsat.int.

The Ocean and Sea Ice Satellite Application Facility (OSI SAF) is producing on an operational basis a range of air-sea interface products, namely: wind, sea ice characteristics, Sea Surface Temperatures (SST), Surface Solar Irradiance (SSI) and Downward Longwave Irradiance (DLI). The sea ice products include sea ice concentration, the sea ice emissivity, sea ice edge, sea ice type and sea ice drift and sea ice surface temperature (from mid 2014).

The OSI SAF consortium is hosted by Météo-France. The sea ice processing is performed at the High Latitude processing facility (HL centre), operated jointly by the Norwegian and Danish Meteorological Institutes.

Note: The ownership and copyrights of the data set belong to EUMETSAT. The data is distributed freely, but EUMETSAT must be acknowledged when using the data. EUMETSAT's copyright credit must be shown by displaying the words "copyright (year) EUMETSAT" on each of the products used. User feedback to the OSI SAF project team is highly valued. The comments we get from our users is important argumentation when defining development activities and updates. We welcome anyone to use the data and provide feedback.

1.2 Scope

This document is dedicated to the OSI SAF product users and describes the scientific background of, and details in, the OSI SAF global reprocessed sea ice concentration products, covering both OSI-409, OSI-409-a and OSI-430.

1.3 Overview

Since the start of the operational production of sea ice products in 2002 the growing user group has brought more focus on expanding the available data set. It was therefore decided to reprocess historical passive microwave data to extend the OSI SAF sea ice concentration data set. This effort was started in 2006 as a part time EUMETSAT visiting scientist activity in collaboration with the UK Met Office. The goal was to reprocess the SSM/I data record. A collaboration was also established with NSIDC to include the SMMR data record in the project, and an EUMETSAT visiting scientist project was set up for this task. The OSI SAF project team and these two Visiting Scientist projects initiated the OSI SAF re-processing and produced a first version of the dataset based on the SSM/I data. Later further improvements have been implemented before the current version was finished. This re-processed product is labelled OSI-409, and covers the period from 1978 to Oct. 2009.

The users of the re-processed sea ice concentration data set has asked for more frequent updates of the re-processed data set. The OSI SAF team therefore decided to set up an off-line production to continuously update the re-processed time series with products processed exactly the same way as the re-processed data set, except that the input data are provided by the normal operational data stream and will be using SSMIS data and operational ECMWF NWP

data. This continuously updated product is labelled OSI-430. In addition, there is a data set that covers the period from end of OSI-409 to start of OSI-430. This products is labelled OSI-409-a. This ATBD describes the details of the re-processed production chain that has been used for these three products/data sets. More details are also available in [RD.2] and [RD.3] , including validation results.

1.4 Glossary

Acronym	Description
AMSR	Advanced Microwave Scanning Radiometer
DMI	Danish Meteorological Institute
DMSP	Defence Meteorological Satellite Program
ECMWF	European Centre for Medium range Weather Forecast
EUMETSAT	European Organization for the Exploitation of Meteorological Satellites
MET	Norwegian Meteorological Institute
NASA	National Aeronautics and Space Administration
NSIDC	National Snow and Ice Data Center
NWP	Numerical Weather Prediction
OSI SAF	Ocean and Sea Ice Satellite Application Facility
RTM	Radiative Transfer Model
SAR	Synthetic Aperture Radar
SMMR	Scanning Multichannel Microwave Radiometer
SSM/I	Special Sensor Microwave/Imager
SSMIS	Special Sensor Microwave Imager Sounder
TBC	To Be Confirmed
TBD	To Be Determined
TBW	To Be Written

1.5 Applicable documents

[RD.1] OSI SAF CDOP-2 Product Requirement Document, v2.5.

[RD.2] OSI SAF Global Sea Ice Concentration Reprocessing Product User Manual (OSI-409), version 1.3. Available at http://osisaf.met.no/docs.

[RD.3] OSI SAF Global Sea Ice Concentration Reprocessing Validation Report (OSI-409), version 1.3. Available at http://osisaf.met.no/docs.

2 Input data

This chapter describes the SMMR, SSM/I and SSMIS satellite data which can be processed by the OSI SAF sea ice concentration algorithm. The algorithm is flexible and it can process several types of microwave radiometer data, also AMSR. Further, the algorithm is using numerical weather prediction (NWP) data for correction of the brightness temperatures prior to calculating the sea ice concentration. The NWP parameter fields are briefly described.

2.1 The SMMR data

The Scanning Multichannel Microwave Radiometer (SMMR) instrument on board the Nimbus 7 satellite operated from October 1978 to August 1987 (Gloersen et al., 1992). The instrument was operated only every second day due to power supply limitations. The instrument had 10 channels from the six Dicke radiometers at five frequencies (6.6, 10.7, 18.0, 21.0, 37.0 GHz) and vertical and horizontal polarization. The scanning across track was ensured by tilting the reflector from side to side while maintaining constant incidence angle on the ground of about 50°. The scan track on the ground formed a 780 km wide arc in front of the satellite (Gloersen and Barath, 1977). Because of the satellite orbit inclination and swath width there is no coverage poleward of 84°. The SMMR instrument is further described in http://nsidc.org/data/docs/daac/smmr_instrument.gd.html. The SMMR data used by OSI SAF was specially prepared by NSIDC through an associated scientist project. The SMMR data set delivered by NSIDC was based on the SMMR data set in the NSIDC archive. More details about the SMMR data set is available in the associated scientist report (Meier, 2008).

Frequency (GHz)	Polarizations	Field of view	
		Along-track	Cross-track
6.6	H,V	148 km	95 km
10.7	H,V	91 km	59 km
18.0	H,V	55 km	41 km
21.0	H,V	46 km	30 km
37.0	H,V	27 km	18 km

Table 1: Characteristics of the Nimbus 7 SMMR channels (Gloersen and Barath, 1977).

2.2 The SSM/I data

The Special Sensor Microwave/Imager (SSM/I) sensors on bord the Defence Meteorological Satellite Program (DMSP) started its record with the F08 satellite on 9. July 1987 shortly before the SMMR ceased to operate on 20. August 1987. The different SSM/I instrument records are summarised in table 2. The SSM/I is a total power radiometer with a conical scan measuring the upwelling radiation from the Earth at a constant incidence angle of about 50deg at 7 different channels. The channels are summarised in table 3. The swath width is about 1400km.

The Special Sensor Microwave/Imager (SSM/I) data set used for this reprocessing was purchased by EUMETSAT from Remote Sensing Systems (RSS) and covers the whole period of available satellites with SSMI/I instruments from 1987 to 2009. We have used the version 6

of the RSS SSM/I data set. The different satellites and covered periods are listed in Table 2.

The SSM/I data were received as antenna temperatures from RSS. These antenna temperatures were converted to brightness temperatures (Tb's) using a software provided by RSS, as described in chapter 4.1.1.

The SSM/I instrument have five low frequency channels similar to SMMR. In addition, two higher frequency channels with twice the sampling rate are available on the SSM/I. The characteristics of these channels are listed in Table 3. The 85GHz channels had a malfunction on F08, so they are only useful starting with the F11 satellite. The F10 has not been used because they are more noisy than F11 and were not needed for a complete coverage.

Satellite	Period covered
F08	Jul 1987 – Dec 1991
F11	Dec 1991 – May 2000
F13	Dec 1995 – Oct 2009
F14	May 1997 – Aug 2008
F15	Dec 1999 – Jan 2013

Table 2: The different satellite missions carrying the SSM/I instrument and the periods they cover.

Frequency (GHz)	Polarizations	Footprint size	
		Along-track	Cross-track
19.35	H,V	69 km	43 km
22.235	V	50 km	40 km
37.0	H,V	37 km	28 km
85.5	H,V	15 km	13 km

Table 3: Characteristics of the different SSM/I channels (from Wentz, 1991).

The RSS SSM/I version 6 data set incorporates geolocation correction, sensor calibration and quality control procedures, as well as inter calibration between the different satellites from overlapping periods. These procedures are documented in the RSS SSM/I User's Manuals (Wentz, 1991; Wentz, 1993; Wentz, 2006).

The RSS SSM/I data set is constrained with a license for use and distribution, and the brightness temperatures on swath format used in the OSI SAF reprocessing product can therefore not be distributed.

In addition, SSM/I data received from UK MetOffice are used to cover the period from October 2009 until January 2013.

2.3 The SSMIS constant incidence angle scanning microwave radiometer satellite data

The SSMIS is a polar orbiting conically scanning radiometer with constant incidence angle

around 50deg and a swath width of about 1700km. It has window channels near 19, 37, 91, and 150GHz and sounding channels near 22, 50, 60, and 183 GHz. The SSMIS temperature sounding channels 1-4 near 50GHz vertical polarization penetrate into the lower troposphere and partially to the surface (Kunkee et al., 2008). The sea ice concentration algorithm is using brightness temperature swath data as input. It is using the 19V, the 37V and the 37H channel data.

The SSMIS data are used from January 2013 and are received through EUMETCast.

2.4 NWP data and radiative transfer model correction

The brightness temperatures (Tb) are corrected explicitly for wind roughening over open water and water vapour in the atmosphere prior to the calculation of ice concentration. The correction is using a radiative transfer model function (RTM) and NWP data. Over areas with both ice and water the influence of open water roughness on the Tb's and the ice emissivity is scaled linearly with the ice concentration. The emissivity of ice is given by standard tie-point emissivities. The correction procedure is described in detail in Andersen et al. (2006B). The NWP model grid points are co-located with the satellite swath data in time and space and a correction to the Tb's is applied. ECMWF ERA 40 data are used for the period from 1978 to 2002, and ECMWF data from the operational model are used from 2002 onwards. A description of the ERA 40 data archive and the reprocessing can be found in Kålberg et al. (2004). These two NWP model data sets are not completely consistent, however the inconsistencies are expected to be small and the residual error is included in the error estimate. So, ERA 40 and ECMWF operational has been used for OSI-409, while ECMWF operational is used for OSI-409-a and OSI-430.

The following prognostic variables are taken from the ECMWF forecast model output: wind speed, 2m air temperature, total column water, total column liquid water.

The representation of atmospheric liquid water column in the NWP data is not suitable to use for Tb correction (see Andersen et al., 2006B). The Tb's are therefore not corrected for the influence of liquid water. It is constrained to zero in the RTM. The RTM is described in Wentz (1997) and in the next section, section 3.

3 Algorithms

This chapter describes all the algorithms and methods used in the three main steps of the daily sea ice concentration calculations; the level 2, level 3 and level 4 calculations. These three setps are illustrated in Figure 1, and details are provided in the following sub sections.

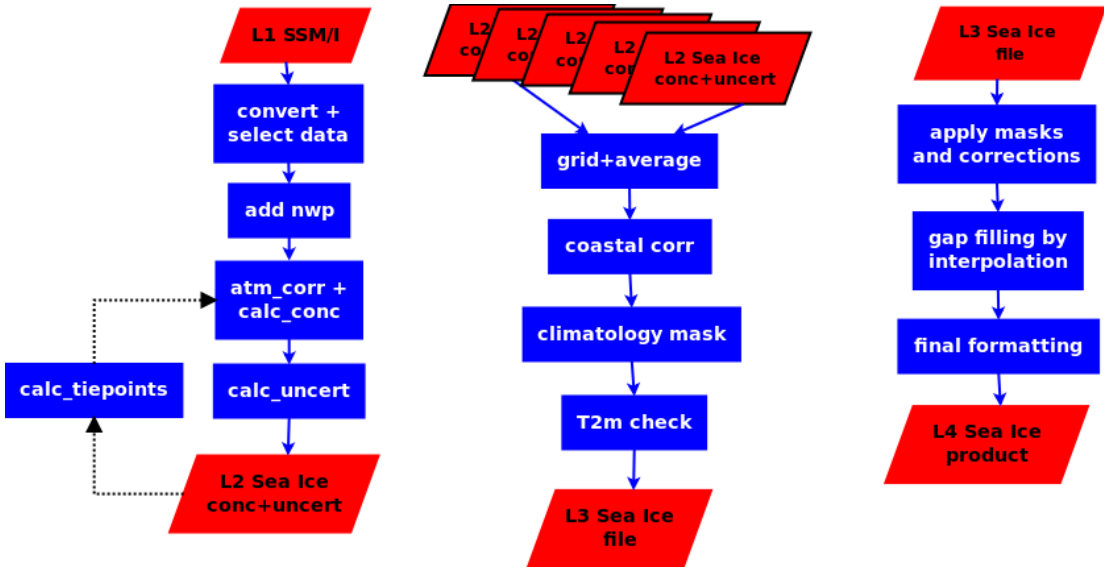

Figure 1: The three main steps in the daily sea ice concentration calculations.

3.1 The ice concentration algorithm

The two ice concentration algorithms are the Bootstrap algorithm in frequency mode (Comiso, 1986; Comiso et al., 1997), and the Bristol algorithm (Smith, 1996). These two algorithms are used in combination as a hybrid algorithm.

3.1.1 Selection of algorithm

When selecting an ice concentration algorithm it is important to ensure low sensitivity to the error sources, including variability in atmospheric emission and surface emission. It is particularly important to find low sensitivity to the parameters which are not corrected for using auxiliary data, such as cloud liquid water in the atmosphere and for ice surface emissivity variability. For climate time series it is important to find an algorithm using the 19 and 37 GHz channels which can be used as far back in time as possible, including the SMMR period from 1978 to 1987 and the first SSM/I (F8) from 1987 to 1991.

The analysis of atmospheric sensitivity in Andersen et al. (2006B) showed that the Bootstrap frequency mode algorithm (Comiso, 1986) had the lowest sensitivity to atmospheric noise over open water. Furthermore, the comparison to high resolution SAR imagery in Andersen et al. (2007) revealed that among the algorithms using the low frequency channels (19 and 37 GHz), the Bristol algorithm (Smith, 1986) had the lowest sensitivity to ice surface emissivity

variability. In addition this algorithm had a low sensitivity to atmospheric emission in particular at high ice concentrations.

Consequently, a hybrid algorithm has been established as a linear combination of two of the tested algorithms, the Bristol algorithm and the Bootstrap frequency mode algorithm. To ensure an optimum performance over both marginal and consolidated ice, and to retain the virtues of each algorithm, the Bristol algorithm is given little weight at low concentrations, while the opposite is the case over high ice concentrations.

3.1.2 The hybrid ice concentration algorithm

The Bootstrap algorithm (Comiso, 1986) is based on the observation of linear clustering of ice Tb's in scatter plots of T_{37v} vs T_{19v} whereas open water Tb's cluster around a single point. It assumes only two surface types: ice and open water, taking into account the variability of both to optimize the detection of small sea ice concentrations. The linear relationship yields the following simple formulation for the total ice concentration, Ct:

$$Ct = (Tb - Tb^W)/(Tb^I + Tb^W) \quad (1)$$

where Tb is the measured brightness temperature, Tb^W is the open water tie-point, and Tb^I is the ice tie-point.

The Bristol algorithm (Smith, 1996) is conceptually similar to the Bootstrap algorithm. In a three-dimensional scatter plot spanned by T_{19v}, T_{37v} and T_{37h} the ice Tb's tend to lie in a plane. The only difference to the Bootstrap algorithm is that instead of viewing the data in the T_{19v}, T_{37v} space, the Bristol algorithm views the data perpendicular to the plane in which the data lies, i.e. in a transformed coordinate system:

$$\begin{aligned} Bristol_x &= T_{37v} + 1.045T_{37h} + 0.525T_{19v} \\ Bristol_y &= 0.9164T_{19v} - T_{37v} + 0.4965T_{37h} \end{aligned} \quad (2)$$

The remaining analysis is identical to the Bootstrap algorithm.

The Bootstrap algorithm is used over open water and the Bristol algorithm is used over ice. At intermediate concentrations up to 40% the ice concentration is an average weighted linearly between the two algorithms. This hybrid algorithm is the OSI SAF sea ice concentration algorithm:

$$\begin{aligned} iceconc &= (1 - wc) * conc_{bristol} + wc * conc_{bootstrap} \\ wc &= (|(t - conc_{bootstrap})| + t - conc_{bootstrap})/(2 * t) \end{aligned} \quad (3)$$

where t is the threshold of 40%.

3.1.3 Tb correction for water vapour and open water surface roughness variability

Using the model function presented in 3.1.4, the Tb's are corrected for the influence of water vapour in the atmosphere and open water surface roughness caused by wind shear. The model function is a semi empirical radiative transfer ocean model describing the Tb as a function of sea surface temperature, surface wind friction velocity, total atmospheric water vapour, total cloud liquid water and surface air temperature. The model function used for SSMIS processing is described in Wentz (1997). The correction procedure is described in Andersen et al. (2006B). At intermediate ice concentrations the surface emission term is a linear combination of ice emissivity derived from tie-point signatures and the open water emissivity derived from the model.

3.1.4 The model function for open water and sea ice

The model function is using the simplified radiative transfer equation, which is adequate for many applications including this one, together with regressions describing the sensitivity to atmospheric and surface parameters. The radiative transfer equation for the top of the atmosphere brightness temperature, F:

$$F(W,V,L) = TBU + \tau[E * TS + (1-E)(\Omega * TBD + \tau * TBC)] \quad (4)$$

where V [mm] is the total water vapour, W [m/s] is the wind speed (at 10m) and L [mm] is the total liquid water in the atmospheric profile (here L=0). E is the surface emissivity, TBC [K] is the cosmic background radiation (2.7K), τ is the atmospheric transmittance, TBU [K] and TBD [K] are the up and down welling atmospheric brightness temperatures. TS [K] is the physical surface temperature and Ω is the reflection reduction factor due to wind induced surface roughness. The subscript i indicates each of the channels 19v, 19h, 37v and 37h. If no i is given, then the quanity is independent of frequency:

$$\begin{aligned} Vertical\ polarization: \Omega_i &= 1 + 2.5 * (\sigma_i^2 - 68 * \sigma_i^6) * \tau_i^2 \\ Horisonal\ polarization: \Omega_i &= 1 + 6.1 * (\sigma_i^2 - 68 * \sigma_i^6) * \tau_i^2 \end{aligned} \quad (5)$$

where the sea surface slope variance, σ is:

$$\sigma_i = \sqrt{(5.22\text{E-}3 * Xi_i * W)} \quad (6)$$

	19V	**19H**	**37V**	**37H**
c0	240.58E+0	240.58E+0	239.55E+0	239.55E+0
c1	305.96E-2	305.96E-2	248.15E-2	248.15E-2
c2	-764.41E-4	-764.41E-4	-438.59E-4	-438.59E-4
c3	885.95E-6	885.95E-6	278.71E-6	278.71E-6
c4	-40.80E-7	-40.80E-7	-3.23E-7	-3.23E-7
c5	0.60E+0	0.60E+0	0.60E+0	0.60E+0
c6	-0.16E+0	-0.16E+0	-0.57E+0	-0.57E+0
c7	-2.13E-2	-2.13E-2	-2.61E-2	-2.61E-2
a0	11.80E+0	11.80E+0	28.10E+0	28.10E+0
av1	2.23E-3	2.23E-3	1.85E-3	1.85E-3
av2	0.00E-5	0.00E-5	0.17E-5	0.17E-5
ε0	162.53E+0	83.88E+0	186.31E+0	101.42E+0
ε1	-25.70E-2	-52.22E-2	-56.37E-2	-85.88E-2
ε2	17.29E-3	18.76E-3	14.81E-3	20.76E-3
ε3	-11.77E-5	-9.25E-5	-2.96E-5	-7.07E-5
ε4	21.62E-1	-14.72E-1	21.23E-1	-17.01E-1
ε5	0.70E-2	0.21E-2	1.17E-2	0.55E-2
ε6	0.45E-1	-0.16E-1	0.41E-1	-0.19E-1
ε7	0.14E-4	-1.10E-4	-0.71E-4	-1.27E-4
M1	0.46E-3	3.01E-3	-0.09E-3	3.91E-3
M2	3.78E-3	7.50E-3	2.38E-3	7.00E-3
Xi	0.688	0.688	1	1
Eice	0.95	0.90	0.93	0.88

Table 4: Model coefficients and constants.

Tvapour is a sea surface temperature which is representative for water vapour in the atmosphere (Eq. 18A in Wentz, 1997), so if the total water vapour column (V) in the atmosphere is less than 48mm then:

$$Tvapour = 273.16 + 0.8337 * V - 3.029\text{E-}5 * \left(V^{3.33}\right) \quad (7)$$

Equations 22-23 in Wentz (1997) are not included here because scattering by liquid water is neglected.

The water surface emissivity is the sum of two components: a specular Fresnel emissivity, E0, and a wind induced roughness emissivity, Ew. The specular emissivity component is given by (Eq. 25 in Wentz, 1997) for each of the channels i:

$$E0_i = \frac{(\varepsilon 0_i + \varepsilon 1_i * t + \varepsilon 2_i * (t^2) + \varepsilon 3_i * (t^3) + \varepsilon 4_i * q + \varepsilon 5_i * t * q + \varepsilon 6_i * (q^2) + \varepsilon 7_i * (t^2}{Ts} \quad (8)$$

where q=Θ-51 and t=Ts-273.16.

The wind induced emissivity over open water where W1=7 and W2=12:

$$\begin{aligned} &For\ W \le 7\mathrm{m}/s : Ew_i = M1_i * W \\ &For\ 7\mathrm{m}/s < W < 12\mathrm{m}/s : Ew_i = M1_i * W + 0.5 * (M2_i - M1_i) * ((W - W1)^2) / (W2 \\ &For\ W \ge 12\mathrm{m}/s : Ew_i = M2_i * W - 0.5 * (M2_i - M1_i) * (W2 + W1) \end{aligned} \quad (9)$$

The open water emissivity as a combination of the plane surface specular Fresnel reflection and the wind induced roughness emissivity:

$$E_i = E0_i + Ew_i \quad (10)$$

The cosmic background radiation, TBC, is 2.7K. Equation 17a in Wentz (1997) is describing the down-welling brightness temperature due to water vapour in the atmosphere, Td:

$$Td_i = c0_i + c1_i * V + c2_i * (V^2) + c3_i * (V^3) + c4_i * (V^4) + c5_i * (Ts - Tvapour) \quad (11)$$

and the upwelling brightness temperature, Tu:

$$Tu_i = TD_i + c6_i + c7_i * V \quad (12)$$

The coefficients A:

$$\begin{aligned} A0_i &= (a0_i / TD_i)^{1.4} \\ Av_i &= av1_i * V + av2_i * (V^2) \end{aligned} \quad (13)$$

The transmitance through the atmosphere along the line of sight, τ:

$$\tau_i = \exp((-1/\cos(\theta)) * (A0_i + Av_i)) \quad (14)$$

and the up-welling atmospheric Tb

$$Tbu_i = Tu_i * (1 - \tau_i) \tag{15}$$

and the down-welling atmospheric Tb

$$Tbd_i = Td_i * (1 - \tau_i) \tag{16}$$

Finally the simplified radiative transfer equation for the brightness temperature from the atmosphere over open water and sea ice covered surfaces:

$$\begin{aligned} Tb_i = Tbu_i + \tau_i * ((1 - Cice) * E_i * Ts + Cice * Eice_i * Ti + \\ (1 - Cice) * (1 - E_i) * (\Omega_i * Tbd_i + \tau_i * TBC) + \\ Cice * (1 - Eice_i) * (Tbd_i + \tau_i * TBC)) \end{aligned} \tag{17}$$

where Ti is the ice effective temperature for each channel and Ts is the physical sea surface temperature. Cice is the sea ice concentration where 0 is open water and 1 is 100% ice.

3.2 Dynamical tie-points

Tie-points are typical signatures of 100% ice and open water which are used in the ice concentration algorithms as a reference. The tie-points are derived by selecting Tb's from regions of known open water and 100% ice. Usually these tie-points are static in time and space, but they can be adjusted to follow the seasonally changing signatures of ice and open water. Static tie-points are prone to be affected by sensor drift, inter sensor calibration differences and climatic trends in surface and atmospheric emission. The data must therefore be carefully calibrated before computing the ice concentrations. Here we use dynamic tie-points, a method that minimizes these unwanted effects, with or without prior calibration.

During winter, in the consolidated pack ice well within the ice edge, the ice concentration is very near 100 % (Andersen et al., 2007). This has been established using high resolution SAR data, ship observations and by comparing the estimates from different ice concentration algorithms. The apparent fluctuations in the derived ice concentration in the near 100% ice regime are primarily attributed to snow/ice surface emissivity variability around the tie-point signature and only secondarily to actual ice concentration fluctuations. In the marginal ice zone the atmospheric emission may be significant. The fluctuations due to atmospheric and surface emission are systematic. In fact, different algorithms with different sensitivity to atmospheric and surface emission compute very different trends in sea ice area on seasonal and decadal time scales (Andersen et al., 2007). This means that not only do the sea ice area have a climatic trend, but the atmospheric and surface constituents affecting the microwave emission are also changing. For example, different wind patterns, water vapour and liquid water concentrations in the atmosphere, snow depth, fraction of perennial ice etc. In an attempt to compensate for the influence of these unwanted trends the tie-points are derived dynamically using a mean of the last 30 days of swath data. A period of 30 days was found to provide tie-points that captured the seasonal changes without much day-to-day variation. The tie-points used in the operational product are also monthly (but static). An example of the difference between 15-days and 30-days tie-points is shown in .

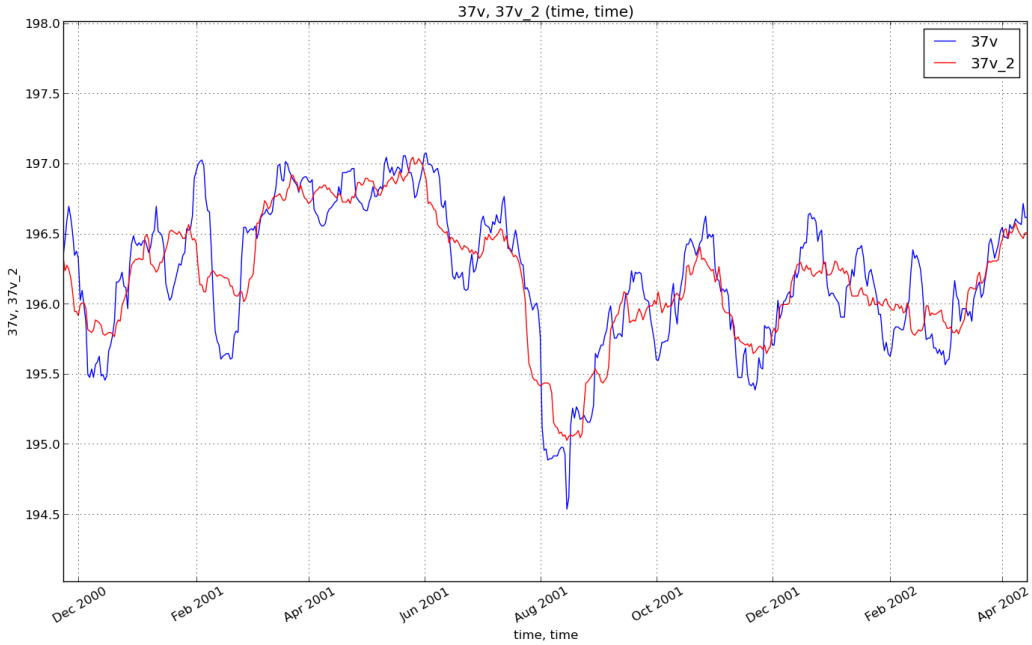

Figure 2: 15-days (blue line) and 30-days (red line) running mean water tie-points for SSM/I F-13 corrected 37V GHz brightness tempeatures.

It is assumed that ice concentrations from the NASA Team algorithm above 95 % are in fact near 100 % ice and that the mean value of these data points can be used to derive the ice tie-point. The NASA Team ice concentration is the initial guess before the iteration and the OSI SAF ice concentration does not depend on the NASA Team ice concentration. The analysis of SAR data in Andersen et al. (2007) from the central arctic showed that during winter there is more than 99% ice cover. During strong ice drift divergence and during the summer there may situations where this is not the case. However, during one month of tie-point data collection we are sure to have captured the situations with near 100% ice cover. The standard deviation of the tie-point is included in the total ice concentration error estimate which is the justification for this assumption.

Geographically, the selection of data for the ice tie-point is limited by excluding regions poleward of 84°. This is due to the limited coverage of the SMMR instrument, and the same constraint has been applied to the SSM/I data for consistency. Regions of open water were used for selecting the water tie-point data (53N to 75N and 65S to 80S). There is no attempt to compensate explicitly for sensor drift or inter-sensor calibration differences between the seven different sensors used in the analysis. The dynamical tie-point method is in principle compensating for these problems in a consistent manner.

Dynamical tie-point algorithm summary:

1. On day D, dynamical tie-points for the OSI SAF algorithm for day D-16 are calculated for uncorrected brightness temperatures (BTs), covering a 30-days period from D-31 to D-1. Dynamical tiepoints are computed separately for the Bootstrap algorithm and the Bristol algorithm and both sets are used by the OSI SAF hybrid algorithm, and includes the number of data points for the ice and the water tie-points, the coordinates for the ice line and for the the water point. These points and lines are illustrated in Figure 3 - Figure 5.

2. For each swath grid point in the data files from day D-16, ice concentrations and corrected BTs are calculated, using uncorrected tie-points for day D-16, NASA team ice concentration (static tie-points, Comiso et al. 1997) as first guess and NWP data in the 3 step interative method of Andersen et al. (2006B).
3. Dynamical tie-points for the OSI SAF algorithm for day D-31 are calculated for corrected BTs, covering a 30-days period from D-46 to D-16. The corrected Bts from step 2 are used.
4. For each swath grid point in the data files from day D-31, ice concentrations and new corrected BTs are calculated, using corrected tie-points for day D-31, NASA team ice concentration (static tie-points, Comiso et al. 1997) as first guess and NWP data in an 3 step interative method.
5. These ice concentrations values based on corrected tie-points and Bts for day D-31 are then used in the further processing.

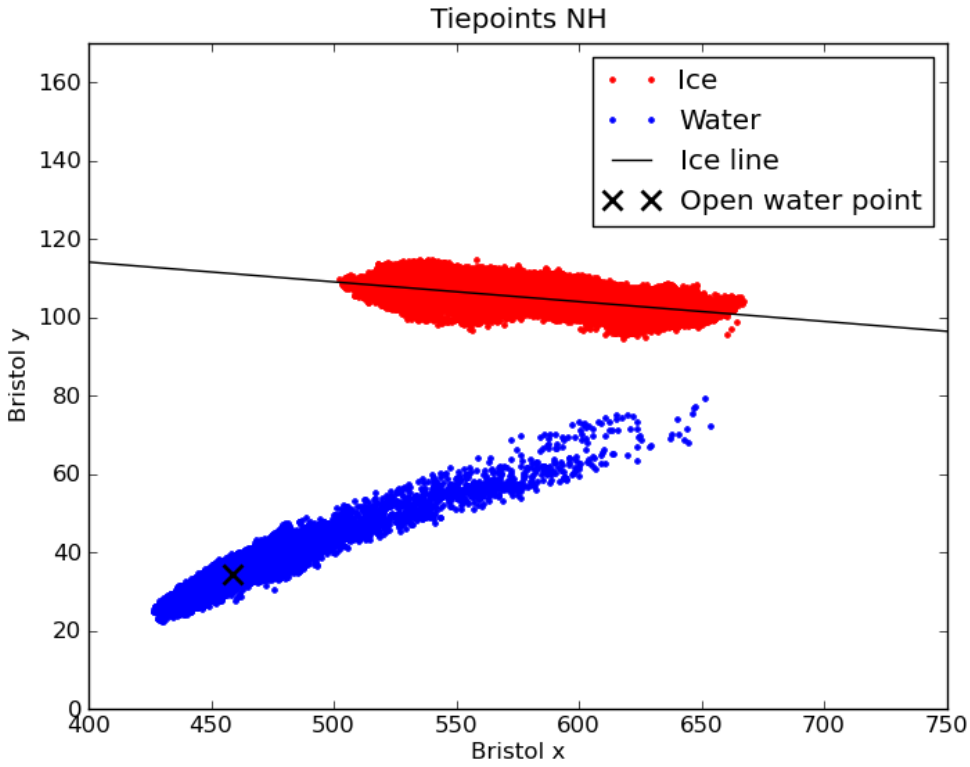

Figure 3: Tie-points derived for the Bristol ice concentration algorithm 3rd Dec 2011, Northern Hemipshere.

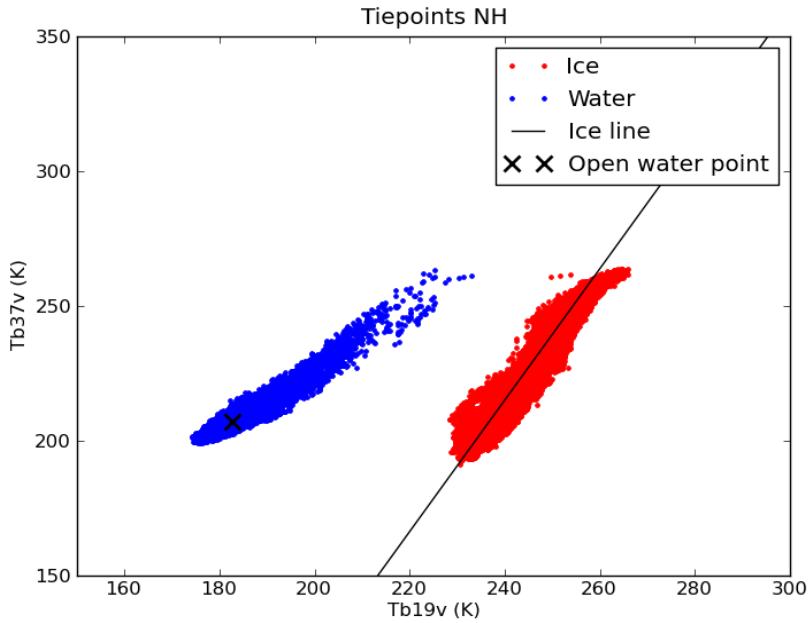

Figure 4: Tie-points derived for the Comiso boot-strap ice concentration algorithm 3rd Dec 2011, Northern Hemipshere.

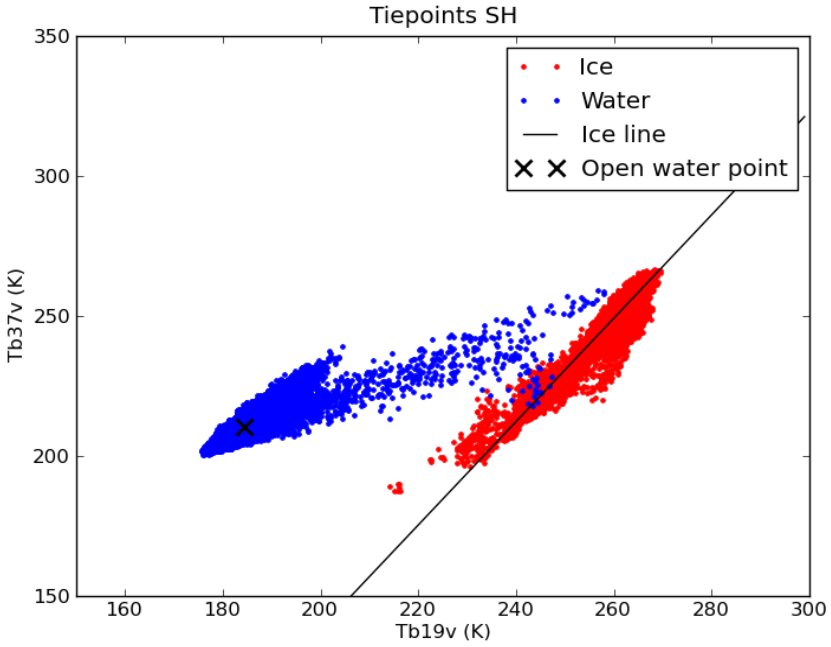

Figure 5: Tie-points derived for the Comiso boot-strap ice concentration algorithm 3rd Dec 2011, Southern Hemipshere.

3.3 Sea ice concentration uncertainties

Uncertainty estimates are needed when the ice concentration data are compared to other data sets or when the ice concentrations are assimilated into numerical models. The mean accuracy of some of the more common algorithms, used to compute ice concentration from SSM/I data, such as NASA Team and Bootstrap are reported to be 1-6 % in winter (Andersen et al., 2006A). This is also achieved with the OSI SAF algorithm.

The polar atmosphere is generally transparent for microwave radiation in between the sounding channels called the atmospheric windows near 19, 37, 90, and 150 GHz. For typical polar atmospheric states the down-welling emission at the surface is about 5-15 K at 18 GHz, 20-40 K at 36 GHz, 30-100 K at 90 GHz. For comparison, the sea ice surface emission is typically 150-260 K. When computing the ice concentration using the atmospheric window channels, the atmospheric emission and scattering is an error source. The tie-points are typical ice and water signatures representative on a hemispheric scale. Deviations from the typical surface emission signatures result in ice concentration uncertainties. The SSM/I and SSMIS instrument has large foot-prints on the ground, and the algorithms with the lowest sensitivity to both atmospheric and surface emissivity variability use Tb's at different frequencies with different foot-print size. Representing these large foot-prints on a finer, predefined grid results in a representativeness error. In addition there is the geo-location error, sensor noise, drift, and sea ice variability over the sampling period.

We make the assumption the total uncertainty σtot can be written as

$$\sigma_{tot}^2 = \sigma_{algo}^2 + \sigma_{smear}^2 \quad (18)$$

where σalgo is the inherent uncertainty of the concentration algorithm, σsmear is the uncertainty due to resampling to a grid where the sensor footprint covers more than one pixel.

3.3.1 Algorithm and tie-point uncertainty

Both the water surface and ice surface emissivity variabilities result in ice concentration uncertainties. Emission and scattering in the atmosphere also affects the Tb's and the computed ice concentrations. Different algorithms have different sensitivities to these surface and atmospheric parameters (Andersen et al., 2006B). Further, both the atmospheric and surface parameters affecting the ice concentration estimates have climatic trends (Andersen et al., 2007). To minimize the uncertainties due to these two parameters, the Tb's are corrected using NWP data for atmospheric humidity and open water roughness in this reanalysis. The dynamical tie-points minimizes uncertainty due to the climatic trends in the atmosphere and on the ice surface on a hemispheric scale while regional trends may still exist.

Ice concentration can be interpreted as a superposition of water and ice

$$iceconc = (1 - \alpha(ic)) \cdot water + \alpha(ic) \cdot ice \quad (19)$$

where ic is the ice concentration calculated by the algorithm. The functional dependency between α and the calculated ice concentration ic is described by:

- $ic \leq 0$, $\alpha=0$

- $0 < ic < 1$, $\alpha = ic$
- $ic \geq 1$, $\alpha = 1$

which can be written as

$$\alpha(ic) = \Pi_{0,1}(ic)\, ic + H(ic - 1) \tag{20}$$

where Πa,b (x) is the Boxcar function and H(x) the Heaviside step function. Using equation 19 and assuming the uncertainty for the ice and water part is independant this leads to a total algorithmic uncertainty as

$$\sigma_{algo}(\alpha(ic)) = \sqrt{(1 - \alpha(ic))^2 \sigma^2_{water} + \alpha^2(ic)\sigma^2_{ice}} \tag{21}$$

where $\sigma_{water} = \sigma(IC(P_{openwater}))$ and open water is determined by a monthly varying ocean mask, IC is the functional mapping of the ice concentration algorithm and Pc denotes the set of swath pixels for all swaths (used calculating the daily product) selected on the condition C.

$\sigma_{ice} = \sigma(IC(P_{ocean,\, nasateam > 0.95}))$ e.g. the standard deviation of the calculated ice concentration of those pixels clear of the coast having a NASA Team concentration > 95%.

3.3.2 Smearing uncertainty

The smear uncertainty is the error due to the sensor footprint covering more than one pixel in the level3 product grid. Foot-print sizes for the channels used for ice concentration mapping range from about 56 km for the 19 GHz channels to about 33 km for the 37 GHz channels. Foot-prints of uneven size are combined in the algorithms when computing the ice concentration. The foot-print ice concentration is represented on a predefined grid. The ice concentration data are normally represented on a finer grid (typically 10 or 25 km) than the sensor resolution (33 to 56km). This is sometimes called smearing. The combination of foot-prints of uneven size in the ice concentration algorithm results in an additional smearing effect. This we call the foot-print mismatch error. The smearing and the foot-print mismatch error can not be estimated separately. However, the combined error can be estimated if all other error sources and the ice cover reference are known *a priori*. It can also be simulated using high resolution ice concentration reference data and a model for the satellite measurement foot-print patterns.

The error is calculated taking a cloud free 1 km MODIS image and assigning ice concentrations to all pixels based on the channel 1 brightness. For each pixel the corresponding brightness temperature is calculated for all relevant microwave channels based on standard tiepoints (Comiso et al. 1997). Using channel specific sensor footprints for weighting the ice concentration is calculated from the 1km brightness temperature image in the specified final resolution i.e. 10, 12, 25 and 50 km. This ice concentration is compared to the MODIS ice concentration regridded to the same resolution. The standard deviation of the difference between these sets of ice concentration values is the standard deviation of the smeared points.

The standard deviation of smeared points is denoted as σsmear (sensor, resolution, algorithm) (abbreviated to σsmear (s, r, a)). As the ice concentration approaches zero or 1 the spatial variation of the ice cover diminishes thus the smearing has less effect. This is reflected in the

scaling:

$$\sigma_{ss}(s,r,a,ic)= \left(\Pi_{0,\sigma_{water}}(ic)\frac{ic}{\sigma_{water}}+\Pi_{\sigma_{water},1-\sigma_{ice}}(ic)+\Pi_{1-\sigma_{ice},1}(ic)\frac{1-ic}{\sigma_{ice}}\right)\sigma_{smear}(s,r,a) \quad (22)$$

The use of scaling thresholds σwater and 1 − σice are somewhat arbitrarily selected.

3.3.3 Uncertainty of OSI SAF ice concentration algorithm

The OSI SAF ice concentration is calculated as a linear combination of the *Comiso* and *Bristol* algorithm which means the total smear uncertainty as

$$ic_{osi}(ic_{comiso},ic_{bristol})=(1-\beta(ic_{comiso}))ic_{comiso}+\beta(ic_{comiso})ic_{bristol} \quad (23)$$

where the scaling factor $\beta(ic_{comiso})$ is

$$\beta(ic_{comiso})=\Pi_{0,\tau}(ic_{comiso})\frac{ic_{comiso}}{\tau}+H(ic_{comiso}-\tau) \quad (24)$$

and τ a threshold value set to 0.4.

3.3.4 Total uncertainty

Using equation 18 the total uncertainty is calculated as

$$\sigma_{total-osi}(s,r,osi,ic)=\sqrt{\sigma^2_{algo-osi}(ic)+\sigma^2_{ss-osi}(s,r,osi,ic)} \quad (25)$$

Since some users have requested that the different uncertainty terms are provided, the reprocessed OSI SAF sea ice concentration product provides these uncertainties:

- total uncertainty $\sigma\, total-osi(s,r,osi,ic)$ (equation 25),
- the algorithmic uncertainty $\sigma\, algo-osi(ic)$ (equation 21),
- the smear uncertainty $\sigma\, ss-osi(s,r,osi,ic)$ (equation 22).

Typical uncertainty values are shown in Figure 6.

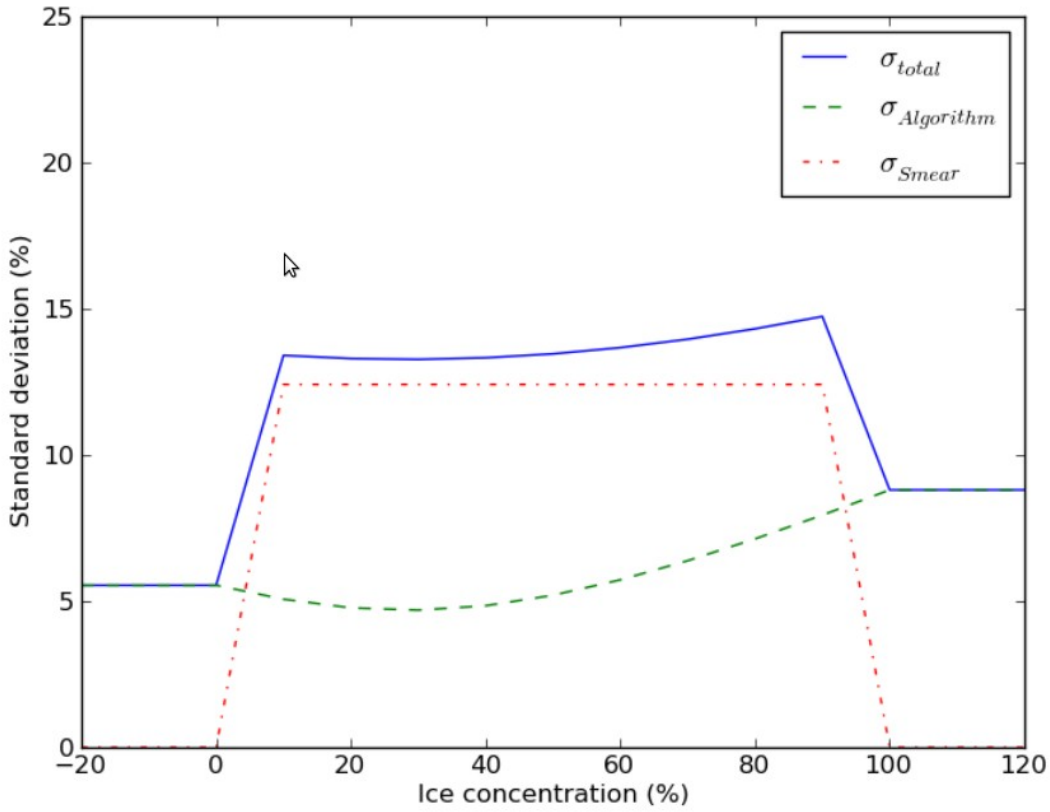

Figure 6: Uncertainty components as a function of ice concentration for the OSI SAF reprocessed ice concentration product .

3.4 Level 3 gridding and daily compositing

The L3 step contains the gridding of the swath data to daily fields, and calculation of corrections and masking fields.

3.4.1 Daily gridding

The daily gridding searches for all satellite observation within 24 hours, centered on 12:00 UTC, and grids these to the final output grid. The observations within one grid cell are averaged, using a weight defined as:

$$weight = 1.0 - (dist / inflrad) * 0.3 \quad (26)$$

where *dist* is the distance between the observation and center of grid point, and *inflrad* is the radius of influence. The influence radius depends on the sampling radius for the channel. For low resolution channels (19, 22 and 37 GHz) 18 km is used and for 85GHz 9 km is used. The 85GHz is kept for internal use, and no ice concentration product based on this sensor is provided.

The gridding is done for all areas with data coverage, including the coastal zone. A gridded field is made for all the ice concentration estimates, based on both uncorrected and corrected brightness temperatures, and for the algorithms present in the L2 files. A similar gridding/averaging is applied for the uncertainty estimates, using the following equation:

$$\begin{aligned} weight &= 1.0 - (dist/rad) * 0.3 \\ SumStd2 &= \sum_{swaths} (ConcStd^2 * weight) \\ SumWeight &= \sum_{swaths} (weight) \end{aligned} \qquad (27)$$

$$error = \sqrt{(SumStd2/SumWeight)}$$

In the averaging, observations from multiple satellite missions are available in overlapping periods. During overlaps in the SSM/I period, observations from different satellites are averaged. The dynamical tie-point approach handles the possible inter satellite differences, which is shown in the validation report [RD.3] .

3.4.2 Coastal correction

Observations in the coastal zone are a mixture between land and water/sea ice. Land has similar signatures to sea ice, and the algorithms therefore overestimate the sea ice concentration in these areas. To correct for these so-called land spill-over effects, an extra coastal correction step has been implemented. The method implemented is described in detail in Cavalieri et al. (1999). In short, this method first calculates monthly average ice concentration for all the months in a selected year and then finds the minimum ice concentration from these averages. This minimum is then used to correct the ice concentration values in the coastal zone if adjacent non-coastal grid points are ice free. The minimum monthly average ice concentration fields were calculated using data from 1985 for SMMR and 1992 for SSM/I. Separate fields were calculated for all algorithms processed.

This processing step generates an additional field with the coastal correction to be added to the concentration field, without applying it.

3.4.3 Climatological maximum extent masking

To mask out erroneous ice outside areas where sea ice is ever likely to occur, a monthly maximum extent climatology has been used. This climatology has been produced by NSIDC using SMMR and SSM/I monthly averaged ice concentrations and finding the maximum extent for each month between 1979 and 2007. A zone of 350 km has been added to the maximum extent NSIDC maps to assure that the masks are surely outside the areas were sea ice is ever likely to occur. Examples of these masks are given in Appendix B. More details about these monthly climatological maximum fields (or ocean mask as called by NSIDC) are available from NSIDC:

http://nsidc.org/data/smmr_ssmi_ancillary/ocean_masks.html.

This processing step collects the respective monthly mask and adds it to the file as a separate

layer.

3.4.4 T2m check

A quality check using the NWP T2m (air temperature at 2 meters) field is used in the processing. The T2m NWP values that have been interpolated in time and space to each observation in the add NWP step, are gridded and averaged to the product grid similar as for the ice concentrations. This field is then added as a separate layer for later use. The test applying the T2m value is based on experience from the operational OSI SAF chain, and shows useful for removing gross errors far from the sea ice edge. In the reprocessing data set it is not used for modifying the nominal value, just mark questionable data.

3.5 Level 4 gap filling by interpolation

This L4 step contains gap filling of some areas with missing data by interpolation, applying masks and coastal corrections, and final formatting to present the final ice concentration product. This section describes the algorithm used for the gap filling by interpolation

3.5.1 Gap filling by interpolation

For easing the use of the reprocessing data set, it was decided that some level of spatial interpolation should be performed for reducing the occurrence of gaps. Only missing data are interpolated. Interpolated data points are clearly marked in the product file (section 5.1.3) so that users can choose to discard them and only ingest retrievals that rely on satellite signal.

Data gaps can occur in several forms, such as missing scan lines, missing orbits and polar observation hole. While spatial interpolation might be efficient in filling small gaps (e.g. one or two missing scan lines), it necessarily blurs the sea ice concentration features. This effect becomes overwhelming when large areas are missing. To overcome this issue, yet implementing a general approach for all cases, the ice concentration estimates from the previous and next daily products are used in the interpolation as well. In the case of SSM/I, it means that interpolation on a given date D uses pixels from 3 data files: D-1, D and D+1.

The interpolated value at grid cell (i,j) for day *D* is given by:

$$X_{i,j}^{D} = K \cdot \left(w_{i,j}^{D-1} \cdot X_{i,j}^{D-1} + w_{i,j}^{D+1} \cdot X_{i,j}^{D+1} + \sum_{k,l} W^{D}(k,l;i,j) X_{k,l}^{D} \right) \quad (28)$$

where X is the sea ice concentration value and K is a normalizing factor given by:

$$w_{i,j}^{D-1} + w_{i,j}^{D+1} + \sum_{k,l} W^{D}(k,l;i,j) = 1/K \quad . \quad (29)$$

From Eq. 28, it is clear that the *spatial* interpolation from neighbors of cell (i,j) only uses values from date *D*, while the *temporal* interpolation is only concerned with the value from the exact (i,j) cell but from dates *D-1* and *D+1*. This strategy ensures that the interpolation will be efficient in the two following extreme scenarios. In a region where we never have satellite observations (e.g. the polar observation hole in the Northern Hemisphere), the spatial interpolation term will be the only contribution. Conversely, in the case of several missing

swath on date D only (nominal coverage on D-1 and D+1), the interpolated values will be computed from the previous and next dates, taking advantage of the persistence of sea ice concentration over such a short period. The interpolation for intermediate cases (when both spatial and temporal neighbors exist) is a compromise of those extreme situations.

In Eq. 28, the weighting parameters are computed as follows:

$$w_{i,j}^{D} = 1/(\sigma_{i,j}^{D})^2 \cdot (2N_{max}+1)$$
$$W^{D}(k,l;i,j) = 1/(\sigma_{k,l}^{D})^2 \times \exp\left(-0.5 \cdot \left(\frac{\Delta(k,l;i,j)}{R_{i,j}}\right)^2\right) \quad (30)$$

where σ is the standard deviation associated to each ice concentration estimate (section 3.3), Δ is the distance between a given (k,l) neighbor and cell (i,j) and R is an auto-correlation radius. The spatial interpolation weight is thus based on an isotropic gaussian shape, and almost all (>99.9%) of the interpolation weight is concentrated inside a [-3R;+3R] x [-3R;+3R] km^2 area, which translates into a [-N_{max};+N_{max}] x [-N_{max};+N_{max}] grid cells square area. It was found that a spatially varying radius R was needed for optimal gap filling and the value R = latitude of (i,j) (in degrees) was taken.

In the case of SMMR which was operated every second day, the interpolation is performed with *D-2* and *D+2* instead of *D-1* and *D+1*.

4 Validation and Technical Aspects

4.1 Error estimates

The product includes a specific error estimate fields, which is described in section 3.3.

4.2 Exception handling

4.2.1 Missing input data

In the case of missing input data, no product will be distributed for those days with complete missing data coverage. For cases with only partial missing coverage, the gap filling routines described in section 3.5 will be applied.

4.3 Algorithm validation

The performance of the algorithm has been validated through the product validation of OSI-409. These validation results are presented in [RD.3] .

4.4 Assumptions and Limitations

The following list mentions assumptions and limitations for the reprocessed sea ice concentration processing chain.

- It is assumed that the SMMR, SSM/I and SSMIS data sets used in this processing, combined with the use of dynamical tie-points, provide a sufficient inter sensor stability for climate purposes.
- The brightness correction scheme used do not take into account the correction for liquid water vapour, as this is not accurately enough in the NWP data used.
- The total uncertainty in each data grid point is assumed to be represented by the algorithm uncertainty and the smearing uncertainty.
- The gap-filling method used is only applied to fill gaps in the daily products were there exist a product for the day before and the day after (for SMMR, two days before and two days after).

5 References

Andersen, S., L. Toudal Pedersen, G. Heygster, R. Tonboe, and L Kaleschke, Intercomparison of passive microwave sea ice concentration retrievals over the high concentration Arctic sea ice. *Journal of Geophysical Research* 112, C08004, doi10.1029/2006JC003543, 2007.

Andersen, S., R. T. Tonboe and L. Kaleschke. Satellite thermal microwave sea ice concentration algorithm comparison. *Arctic Sea Ice Thickness: Past, Present and Future*, edited by Wadhams and Amanatidis. Climate Change and Natural Hazards Series 10, EUR 22416, 2006A.

Andersen, S., R. Tonboe, S. Kern, and H. Schyberg. Improved retrieval of sea ice total concentration from spaceborne passive microwave observations using Numerical Weather Prediction model fields: An intercomparison of nine algorithms. *Remote Sensing of Environment, 104, 374-392*, 2006B.

Comiso J.C, D.J. Cavalieri, C.L. Parkinson, and P. Gloersen. Passive microwave algorithms for sea ice concentration: A comparison of two techniques. *Remote Sensing of Environment* 60, 357-384, 1997.

Comiso J.C. Characteristics of arctic winter sea ice from satellite multispectral microwave observations. *Journal of Geophysical Research* 91(C1), 975-994, 1986.

Gloersen, P., and F. T. Barath. A scanning multichannel microwave radiometer for Nimbus-G and SeaSat-A. *IEEE Journal of Oceanic Engineering OE-2*(2), 172-178, 1977.

Gloersen, P., W. J. Campbell, D. J. Cavalieri, J. C. Comiso, C. L. Parkinson, H. J. Zwally. Arctic and Antarctic sea ice, 1978-1987: satellite passive-microwave observations and analysis. *NASA SP-511*, Washington D. C., 1992.

Kunkee, D. B., G. A. Poe, D. J. Boucher, S. D. Swadley, Y. Hong, J. E. Wessel, and E. A. Uliana, 2008. Design and evaluation of the first special sensor microwave imager/sounder, IEEE Trans. Geo. Rem. Sens. 46(4), 863-883.

Kålberg, P., A. Simmons, S. Uppala, and M. Fuentes. The ERA-40 archive. *ERA-40 Project Report Series*, ECMWF, Reading, 2004.

Meier, W. Scanning Multichannel Microwave radiometer (SMMR) reprocessing for EUMETSAT. *OSI SAF Visiting Scientist Report*. 9 pages, 2008.

Smith, D. M. Extraction of winter total sea ice concentration in the Greenland and Barents Seas from SSM/I data. *International Journal of Remote Sensing 17*(13), 2625-2646, 1996.

Wentz, F. J. A model function for ocean microwave brightness temperatures. *Journal of Geophysical Research 88*(C3), 1892-1908, 1983.

Wentz, F. J. A well-calibrated ocean algorithm for SSM/I. *Journal of Geophysical Research* 102(C4), 8703-8718, 1997.

Wentz, F. J. User's Manual, SSM/I Antenna Temperature Tapes, Revision 1. *RSS Technical Report 120191,* 1991.

Wentz, F. J. User's Manual, SSM/I Antenna Temperature Tapes, Revision 2. *RSS Technical Report 120193,* 1993.

Wentz, F. J. User's Manual, SSM/I Antenna Temperature, Version 6. *RSS Technical Memo 082806*, 2006.